Journal of Engineering Science and Technology
23rd EUREKA 2025 Special Issue February (2026) 110 - 122

THERMAL DISTRIBUTION OF A HYDROGEN TANK DURING REFUELLING FOR HEAVY-DUTY APPLICATIONS

WONG KHAI EE, NOOR ZAFIRAH ABU BAKAR*, KU PEI XUAN

School of Engineering, Taylor's University,
No. 1 Jalan Taylor's, 47500, Subang Jaya, Selangor DE, Malaysia
*Corresponding Author: noorzafirah.abubakar@taylors.edu.my

Abstract

Hydrogen as a fuel is one of the cleanest available sources of energy, with its only emission being pure water. However, it has a low volumetric energy density, which means that extremely high pressures are required during the refuelling process. High-pressure refuelling causes uneven thermal distribution within the tanks, causing hotspots and creating potential weak points in the tank. This study aims to develop validated CFD models of hydrogen refuelling process and analyse the thermal distributions and their flow characteristics. The simulations were conducted at three test conditions with different ambient temperatures but at constant hydrogen temperature and pressure ramp rate. The study found that a significant factor in managing a hydrogen tank's temperature during refuelling is controlling the internal flow behaviour by changing the tank inlet design. The three modified designs are the straight pipe, perforated pipe, and extended perforated pipe. The most effective design was the extended perforated pipe design, which significantly improves thermal safety by distributing the cold hydrogen evenly throughout the tank. This design prevented the formation of severe hot spots, achieving a 38% reduction in maximum temperature compared to the original design. By manipulating the flow in this way, the refuelling process becomes safer and more efficient.

Keywords: CFD, Hydrogen, Hydrogen refuelling, Hydrogen tank.

1. Introduction

Based on the findings from the United States Environmental Protection Agency, greenhouse gas emissions from the mobility sector account for nearly 29% of the total emissions in the country [1]. The United Nations has also found that the mobility sector accounts for approximately a quarter of the total carbon emissions in the world [2]. This information has made the mobility sector one of the main causes of climate change. As there are many global climate goals, such as the Sustainable Development Goals (SDG) and the Paris Emissions Agreement, which all call for a drastic reduction in carbon emissions, alternative powertrain systems and fuels have been introduced in order to meet these goals. These technologies have varying working principles and have different advantages and limitations.

One of these technologies that has been implemented at a large scale would be start-stop technology. It is present in almost all modern vehicles, starting from the early 2000s. The system would turn off the engine while the vehicle is at a complete stop, reducing its idling time [3]. However, this would place a strain on the battery and the components to start the engine, reducing its lifespan [4]. This is also not applicable to the heavy-duty vehicles used in the mobility sector, as the idle times of these vehicles are shorter than average, which reduces the effect of the reduction in carbon emissions [5].

Hybrid vehicles are also gaining in popularity and is easily accessible, with many car models offering the powertrain option alongside the traditional engine option. It has an additional electric motor being used alongside the engine, with varying configurations being the engine only acting as a generator for the electric motor or the engine turning on when at higher vehicle speeds [6]. However, these vehicles still have a reliance on fossil fuels and emit carbon dioxide.

Fully electric vehicles (EVs) and alternative fuel vehicles are technologies that have zero direct carbon emissions. EVs have been gaining popularity rapidly, especially for users who drive daily in cities where there is heavy traffic often and short commutes. Electric vehicles have the same consumption of electricity on average, even in start-stop traffic, while vehicles with internal combustion engines (ICE) experience higher fuel consumption in the same scenario.

However, EVs have a much longer charging duration, with an average of around 3 hours. This duration would be even longer for heavy-duty vehicles, where there are larger motors and batteries present [7]. Moreover, many developing countries still use non-renewable energy sources to generate electricity, which would mean that more EVs would still increase carbon emissions [8]. This has also not taken into account the large number of heavy metals used to create the battery components of the electric vehicle [9].

Alternative fuels such as hydrogen and alcohol have been developed to replace the current fuel sources. Alcohol has three times the heat of evaporation when compared to gasoline, which would translate to a generally cooler engine when it is running [10]. With a lower running temperature, the engine is more efficient with reduced energy losses due to heat. Alcohol as a fuel has been readily available in certain parts of the world, sold alongside petrol and diesel.

However, alcohol fuels have a corrosive property, which can erode the metal that the engine is made of [11]. The fuel system would also be clogged as ethanol can dislodge deposits within the pipes, clogging up the filter and injector systems

[12]. Alcohol fuels also still emit carbon dioxide, however at much lower rates when compared to traditional fuels.

Hydrogen as a fuel has zero carbon emissions, as the only byproduct of its combustion is pure water. This property makes it one of the best solutions to the carbon emissions problem. It also has a high gravimetric energy density compared to other fuels, meaning it can provide a high amount of energy per unit of its mass [13]. This is crucial for the mobility sector as the weight of fuel is drastically reduced. Rapid refuelling is also possible with hydrogen, with the process being able to match the speed of refuelling traditional fuels, making it more viable than electric vehicles (EVs) for the mobility sector, where time is of the essence [14].

However, hydrogen has a very low volumetric energy density, meaning that there is a low amount of energy per volumetric unit. This would pose a few challenges, as high pressures would be needed for its storage vessels in order to make it feasible as a fuel for vehicles. A maximum of 350 bar is set for the heavy-duty application tanks, commonly used for the mobility sector.

The refuelling process would need to be carefully managed, as high pressures such as this could cause excessive heating within the tank. The maximum temperature allowed within the tank is 85°C, as any higher could cause material degradation of the tank and cause it to fail prematurely [15]. Measures such as pre-cooling the hydrogen or the tank have been proven to reduce the overall temperature, however systems like these would increase the complexity and cost of their storage and refuelling process [16, 17].

In order to solve these issues, this study aims to create a hydrogen storage tank with improved thermal distribution. 2D Computational Fluid Dynamics (CFD) models would be developed to provide detailed data of the thermal distribution and flow behaviour within the tank during the refuelling process. This would also allow for hotspots to be identified and the impact of variables that are present in the refuelling process. These variables would be the ambient temperature, the hydrogen temperature, and the pressure ramp rates of the refuelling process.

The simulation results were compared with the findings of another study [18], which used real-world experiments and a simple 0D model, for data validation purposes. The validated CFD model would be able to provide comprehensive visualisations, which would allow for improved storage tanks with improved thermal distribution to be designed.

2. Methodology

The methodology of this study consists of several sequences and iteration steps. The first step was to create the geometry of the hydrogen tank. Then, the geometry was discretized, and the setup for the CFD simulation was established. These steps were iterated until the mesh achieved grid independence, and the results were validated.

2.1. Geometry

The tank model was based on COMET Type III hydrogen storage cylinder. The dimensions of the tank were taken from [18] as listed in Table 1, and the actual figure of the tank is shown in Fig. 1.

Table 1. Tank geometries [18].

Inner volume	320 litres
Outer diameter	417 mm
Outer length	3128 mm
Inlet valve diameter	6 mm

Fig. 1. Comet type III hydrogen storage cylinder [18].

Since the tank was axisymmetric, only half of the 2D geometry was designed. This allowed the model to be more computationally efficient while maintaining its accuracy. The tank consisted of three domains: composite, liner, and hydrogen gas. The detailed dimensions of these domains are shown in Fig. 2. The thickness of the liner and composite was not provided, so it was assumed that the liner was 3 mm thick and the composite was 20 mm.

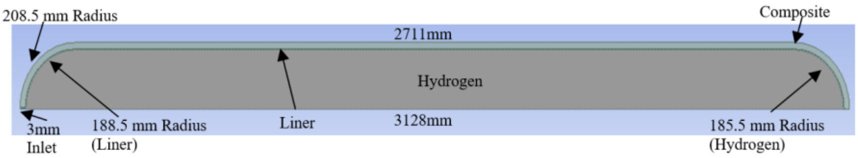

Fig. 2. 2D model.

The material properties of the liners and composite are listed in Table 2.

Table 2. Material properties of the liners and composite [18].

	Liner	Composite
Material	Aluminium	Carbon Fibre Reinforced Polymer
Density (kg/m^3)	2700	1494
Specific Heat Capacity (J/kg.K)	900	938
Thermal Conductivity (W/m.K)	202	1

2.2. Meshing

The domains were discretized with different body sizes to achieve the optimized accuracy and computational time. Table 3 lists the mesh type and the finalized body size, and the number of nodes for the respective domains. Figure 3 shows the close-up view of the mesh at the inlet area.

Table 3. Tank domains mesh details.

Domains	Mesh type	Element size (mm)
Hydrogen	Mix (Tet and Hex)	4
Liner	Mix (Tet and Hex)	1
Composite Casing	Mix (Tet and Hex)	2

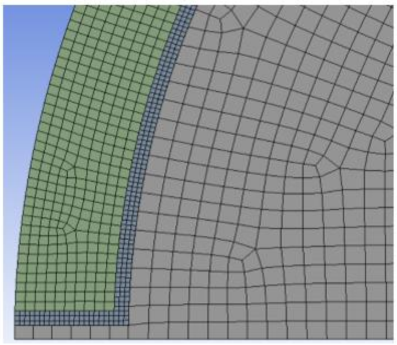

Fig. 3. Section of the meshing at the inlet area.

2.3. Solver setup

Three test conditions were simulated based on the experiment conducted by Klopčič et al. [18]. The ambient temperatures were varied while the hydrogen temperature and the pressure ramp rate were held constant at 25°C and 65 bar/min, respectively. The summary of the test conditions is tabulated in Table 4.

Table 4. Test conditions [18].

Test No.	Ambient Temperature (°C)	Hydrogen Temperature (°C)	Pressure Ramp Rate (bar/min)
1	-15	25	65
2	15	25	65
3	35	25	65

The Energy Equation was enabled to simulate the thermal conductivity of the model. The viscosity model used was the k-omega GEKO equation [19], as it was optimised for this specific purpose. The equation of state used for the density of hydrogen. The thermal conductivity and viscosity properties are set as polynomials, as these properties vary as the temperature increases. The initial tank pressure was set at 30 bar, and the inflow rate was set in terms of mass flow rate. The temperature of the hydrogen was set at the inlet, and the ambient temperature was set at the external wall of the carbon fibre composite. An adiabatic wall was set at the part of the liner where it extended to the inlet. This was done in order for the model to be more stable.

As the flow was highly compressible, the numerical time scheme chosen was a second-order implicit time-stepping scheme. The second-order was chosen as it provided more accurate results by using more derivatives during its approximation process and an implicit scheme for more stable calculations, as there would be large pressure changes [20]. The solving method used was the PISO method, which was designed specifically for this purpose [21]. The size of the timestep used was 0.05 seconds, as this provided accuracy while ensuring the simulation was computationally efficient [22] with the residual values of 10^{-5}.

3. Results and Discussions

This section consists of three main parts. The first part presents the comparison of the simulation results of the original tank design with the measured experimental data to validate the simulation models. The second part is the discussion on the flow characteristics and thermal distribution of the original design. The last part is the presentation of the improvement of the tank inlet designs with their respective flow characteristics and thermal distribution during refuelling.

3.1. Validation results

Figure 4(a) shows the trend of the simulated average temperature inside the hydrogen tank against the refuelling time while Fig. 4(b) shows the experimental trend. The simulation trends do not follow experimental trends at the initial stage of refuelling. However, the simulation trends demonstrate a similar trend to the experiment trends starting at 70 s, when the temperature starts to increase to the maximum value.

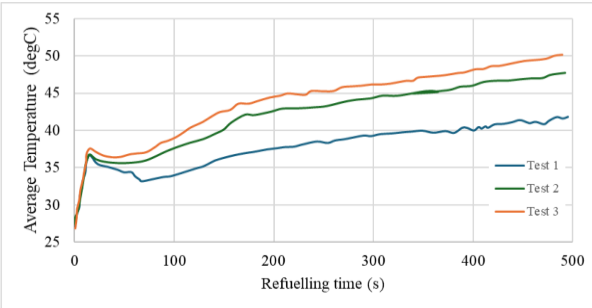

(a) Simulation trend

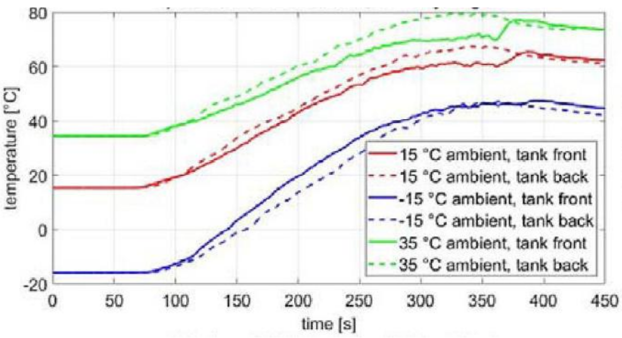

(b) Experimental trend

Fig. 4. Hydrogen temperature against the refuelling time [18].

According to Klopčič et al. [18], the desired refuelling time for the pressure ramp of 65 bar/min was five minutes. At the 5-minute refuelling time, the experiment achieved the maximum temperature, while for the simulation, the maximum temperature was achieved about three minutes later. Table 5 tabulates the temperature difference between the simulation and experiment at the 5-minute refuelling time and the maximum temperature difference.

Table 5. Temperature difference between simulation and experimental data.

Test No.	Simulation		Experiment	% Difference	
	Temp at 5-min (°C)	Max temp (°C)	Temp at 5-min and max temp (°C)	At 5-min	Max temp
1	39.12	41.85	45.40	13.82	7.82
2	43.88	47.85	63.50	30.90	24.65
3	46.18	50.85	75.15	38.55	32.34

The percentage differences increase as the ambient temperature increases. The main reasons for these discrepancies are because of some assumptions were made during the domains modelling, solver setup, and positions of the sensors for the post-processing due to insufficient information. Nevertheless, the simulation models were able to follow the temperature increase trend during the refuelling and produced reliable results with reasonable percentage differences compared to the experimental data. Thus, the simulation models were considered validated.

3.2. Thermal distribution and flow characteristics during refueling for original tank design

The thermal distribution and the velocity streamlines that represent the hydrogen flow characteristics within the original tank design at different stages of refuelling are shown in Figs. 5 and 6, respectively. The thermal distribution and the flow characteristics exhibit similar trends for all test conditions. The difference is only in the magnitude values. Thus, only one test condition was selected for discussion.

At the early stage of the refuelling, as shown in Fig. 5(a), the temperature field displays a non-uniform thermal distribution where it has a cooler region at the midsection and relatively hotter at other areas. In Fig. 6(a), it is observed that there are strong recirculation zones near the inlet. The flow is highly unsteady, with multiple vortices spreading hydrogen into the tank. At this early stage, it can be deduced that the hydrogen flow is highly unstable and mixes strongly, causing a non-uniform thermal distribution with a localized cooling region.

At refuelling time of 150 s, where the temperature increases rapidly, the thermal gradient becomes more visible as shown in Fig. 5(b). The inlet becomes the coldest region while the rear region heats up. This reflects the compressive heating and accumulation of hydrogen, while the inlet still benefits from the low temperature of the incoming gas. In terms of the flow characteristics shown in Fig. 6(b), the flow becomes more organized, with streamlines extending along the tank's length. Flow recirculation is still visible; however, the hydrogen is more uniformly transported downstream toward the rear area.

At the end of the refuelling, the thermal gradient is more distinct as displayed in Fig. 5(c). The rear tank remains the hottest region due to continuous compression heating and reduced mixing, as the tank approaches a quasi-steady state. In Fig.

6(c), the flow is now more streamlined and nearly fully developed along the tank length. Hydrogen fills the tank in an orderly manner.

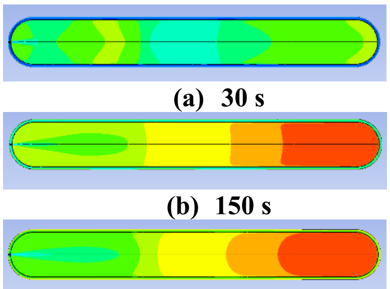

(a) 30 s

(b) 150 s

(c) 300 s

Fig. 5. Thermal distribution.

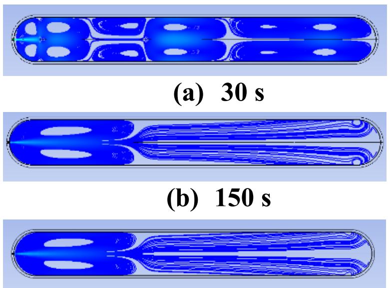

(a) 30 s

(b) 150 s

(d) 300 s

Fig. 6. Hydrogen flow characteristics.

The original tank design shows that at the end of the refuelling, it was able to contain a stable hydrogen flow but with persistent thermal stratification, where the hydrogen is cooler near the inlet and hotter at the rear region. The localized hotspot is critical for safety and efficiency considerations, since excessive temperature rise can affect tank material limits and refuelling rates. Therefore, the inlet requires design improvement to produce a more uniform thermal distribution within the tank and reduce the temperature during refuelling.

3.3. Tank inlet design improvement

Figure 7 displays the close-up views of three modified tank inlet designs and the original design. The original tank design inlet shown in Fig. 7(a) does not include any sort of internal nozzle into the tank, only the external nozzle. Therefore, the inlet is connected directly to the tank.

The first design modification is a straight pipe nozzle shown in Fig. 7(b). The straight pipe nozzle was extended 271 mm into the tank, or approximately 10% of the length of the tank. The inlet diameter of the tank was not changed, remaining at 6 mm. Figure 7(c) displays the second design modification, a perforated pipe nozzle. The nozzle was extended 271 mm into the tank. The inlet diameter of the tank was not changed, remaining at 6 mm. The perforations were 5 mm in length, with 5 mm in between each. There were three clusters of perforations, with the first being 61 mm from the main tank and three in this cluster.

The second cluster was 35 mm from the first cluster, and there were four in this cluster. The final cluster was also 35 mm from the second cluster, and there were eight in this cluster. The last design modification is an extended perforated pipe as shown in Fig. 7(d). The nozzle pipe was extended 2941 mm into the tank. The inlet diameter of the tank did not change, remaining at 6 mm. The perforations were 25 mm in length, and 50 mm in between each. The first perforation starts 61 mm from the inlet, and the pattern was constant throughout. At the final gap, the diameter of the nozzle is dropped to 1mm, at an angle of 21°.

For all the modified designs, the nozzle pipe material was not taken into account for this study. Thus, only a void cutout was done, with all pipe interfaces was set adiabatic.

Figures 8 to 10 illustrate the flow characteristics transition from the initial stage of the refuelling (40 s) to the temperature increment during refuelling (150 s), and to the end of refuelling (300 s) for all four tank inlet designs. The flow was taken during Test 3 condition.

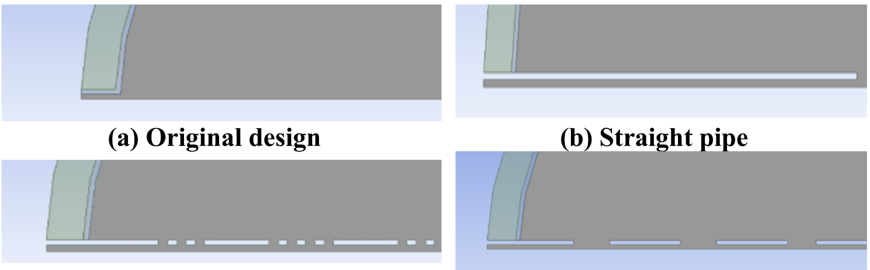

(a) Original design **(b) Straight pipe**

(c) Perforated pipe **(d) Extended perforated pipe**

Fig.7. Comparison of different tank inlet designs.

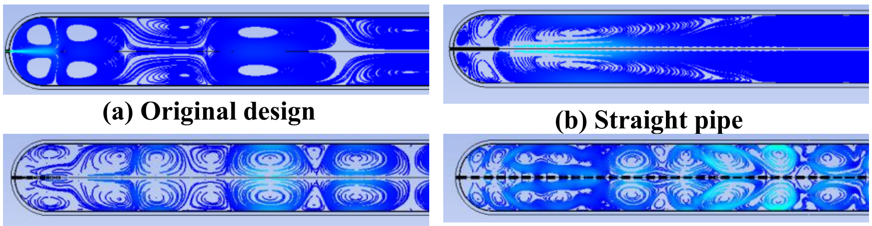

(a) Original design **(b) Straight pipe**

(c) Perforated pipe **(d) Extended perforated pipe**

Fig. 8. Hydrogen flow characteristics at 40 s of refuelling time.

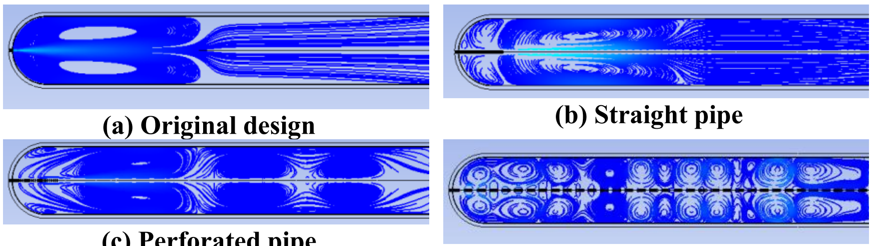

(a) Original design **(b) Straight pipe**

(c) Perforated pipe **(d) Extended perforated pipe**

Fig. 9. Hydrogen flow characteristics at 150 s of refuelling time.

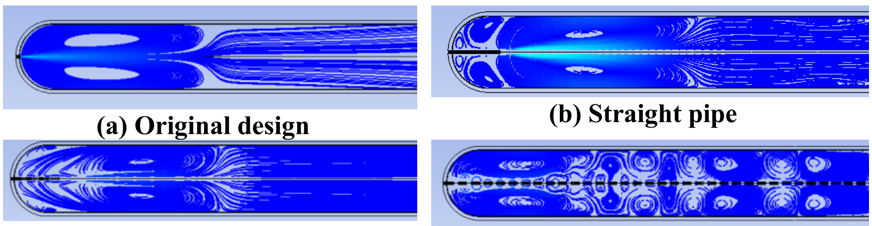

(a) Original design **(b) Straight pipe**

(c) Perforated pipe **(d) Extended perforated pipe**

Fig. 10. Hydrogen flow characteristics at 300 s of refuelling time.

For the original design, the flow transits from a high-velocity, vortex-dominated flow at 40 s, to a more streamlined, elongated flow at 150 s, and finally to a low-velocity, near-stagnant state at 300 s. The initial chaotic mixing gives way to a more stable, less dynamic flow. For the straight pipe design, the flow moves from a centrally focused jet at 40 s to a long, streamlined axial flow at 150 s, and then to a very slow, parallel flow at 300 s. The transition is marked by a steady decrease in velocity and a stabilization of the central flow path.

For the perforated pipe design, the flow starts with multiple, smaller, and well-distributed vortices at 40s. These vortices gradually diminish, and the flow becomes more uniform across the tank at 150s. By the 300 s, the flow is very stable and evenly distributed, indicating efficient filling. For the extended perforated pipe design, the flow maintains a high degree of flow distribution from the start. The transition is characterized by a gradual decrease in velocity while preserving the even distribution of flow. It shows the least amount of change in its pattern and can maintain a uniform flow throughout the refuelling process.

Figure 11 shows the thermal distribution for the respective design at the end of refuelling time (300 s). The thermal distribution is consistent with the flow characteristics of the inlet designs.

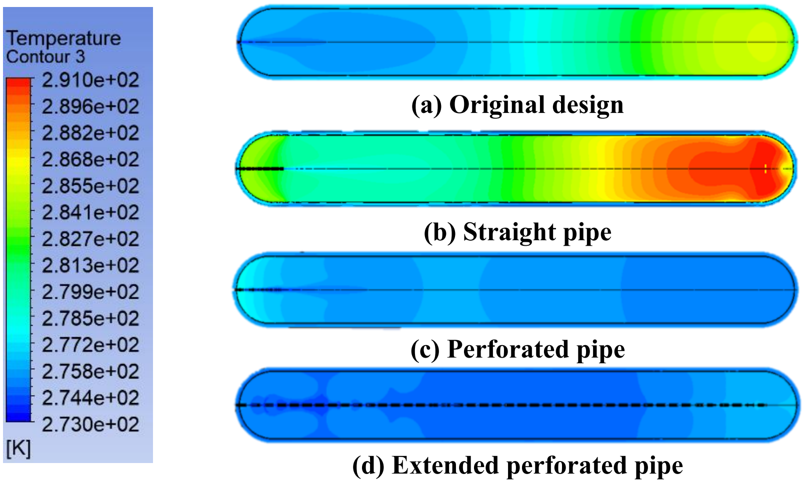

Fig. 11. Thermal distribution comparison between different tank inlet designs.

For the original design (Fig. 11(a)), the hydrogen shows a distinct thermal gradient, with a cool region near the inlet and a significant hot spot at the rear area. The incoming hydrogen forms a single, high-velocity jet that travels towards the tank's far end. This jet's kinetic energy is converted into thermal energy upon impact, creating the large hot spot. The subsequent vortices and recirculation patterns are strong, but not strong enough to completely mix the heat throughout the entire tank, leading to the observed thermal stratification. The continuous influx of cold hydrogen at the inlet keeps that end of the tank at a lower temperature.

The straight pipe design (Fig. 11(b)) exhibits the most pronounced thermal gradient and the highest temperature hot spot at the far end of the tank. The straight pipe concentrates the hydrogen flow into a focused, high-speed jet that travels along the central axis and directly impacts the tank's far end. This concentrated impact results in a very high rate of compression and friction, leading to a much more intense and localized hot spot compared to the original design. The flow remains largely segregated from the outer walls until it reaches the end, which limits heat dissipation and reinforces the extreme temperature difference.

The temperature distribution is much more uniform for the perforated pipe design (Fig. 11(c)) , and significantly cooler overall compared to the original and straight pipe designs. There are no major hot spots observed. The perforated pipe disperses the incoming hydrogen through multiple small holes. This prevents the formation of a single, powerful jet and instead creates numerous smaller, low-velocity jets. The flow's kinetic energy is distributed over a larger area, which greatly reduces localized heating. This distributed flow promotes more even mixing and enhanced heat exchange with the tank's interior surfaces, leading to a much lower and more uniform final temperature.

The extended perforated design (Fig. 11(d)) shows the most uniform and lowest overall temperature profile. The tank remains predominantly cool, with minimal temperature gradients. By extending the perforated pipe over a greater length, this design maximizes the distribution of the incoming flow. The hydrogen is discharged slowly and evenly along the entire length of the tank. This maximizes the available surface area for heat transfer to the tank walls, effectively preventing any significant compression heating or localized hot spots. The result is a highly efficient thermal management system that maintains a cool and consistent temperature throughout the refuelling process.

Table 6 shows a comparison of the maximum temperature difference between the modified designs and the original design for Test 3. The original tank design had a maximum temperature of 46.1°C, which was used as a benchmark for the other designs. There is a minimal difference in temperature for the straight pipe design, which had a maximum of 46.1°C, a difference of only 5%. The perforated pipe design yielded a much better result, a maximum temperature of 33.2°C, which is a significant 28% reduction from the original. The extended perforated pipe design recorded the best results, a maximum temperature of 28.5°C, which is a difference of 38.2%. This shows the best possible design would be the extended perforated pipe design, with the next recommended design being the perforated pipe design.

Table 6. Comparison of maximum temperatures between tank inlet designs.

Nozzle Design	Maximum Temperature (°C)	Difference (%)
Original	46.1	-
Straight Pipe	43.8	5
Perforated Pipe	33.2	28.0
Extended Perforated Pipe	28.5	38.2

4. Conclusions

In conclusion, this study has successfully developed 2D CFD models of the hydrogen refuelling process that were validated. It was identified that the significant issues with the current tank design were highly uneven thermal distributions and hotspots, mostly located at the rear of the tank. The most significant factor in managing a hydrogen tank's temperature during refuelling is controlling the internal flow behaviour by changing the tank inlet design. The three modified designs are the straight pipe, perforated pipe, and extended perforated pipe. The most effective solution was the extended perforated pipe design, which significantly improved thermal safety by distributing the cold hydrogen evenly throughout the tank. This design prevented the formation of severe hot spots, achieving a 38% reduction in maximum temperature compared to the original design. By manipulating the flow in this way, the refuelling process becomes safer and more efficient, directly improving the technical feasibility of hydrogen as a clean energy source.

Abbreviations

0D	0 Dimensions
2DCAD	2-Dimensional Computer Aided Design
CFD	Computational Fluid Dynamics
EV	Electric Vehicle
GEKO	Generalized k-ω Two-Equation Turbulence Model
ICE	Internal Combustion Engine
PISO	Pressure-Implicit with Splitting of Operators
SDG	Sustainable Development Goals

References

1. EPA. (2023). EPA Automotive trends report: greenhouse gas emissions, fuel economy and technology since 1975. In EPA automotive trends report. Retrieved August 30, 2025, from https://nepis.epa.gov/Exe/ZyPDF.cgi?Dockey=P10191WZ.pdf
2. UN. (2021) Fact sheet climate change. Retrieved August 30, 2025, from https://www.un.org/sites/un2.un.org/files/media_gstc/FACT_SHEET_Climate_Change.pdf
3. Bishop, J.; Nedungadi, A.; Ostrowski, G.; Surampudi, B.; Armiroli, P.; and Taspinar, E. (2007). An engine start/stop system for improved fuel economy (No. 2007-01-1777). *SAE technical paper*.
4. Windover, P.R.; Owens, R.J.; Levinson, T.M.; Laughlin, M.; and Gaines, L. (2015). *Stop and restart effects on modern vehicle starting system components* (*No. ANL-15/04*). Argonne National Lab.(ANL), Argonne, IL (United States).
5. Calcagno, J.A. (2005). *Evaluation of heavy-duty diesel vehicle emissions during cold-start and steady-state idling conditions and reduction of emissions from a truck-stop electrification program*. Doctoral Dissertation. University of Tennessee.
6. Overington, S.; and Rajakaruna, S. (2012). Review of PHEV and HEV operation and control research for future direction. *Proceedings of the 3rd IEEE International symposium on power electronics for distributed generation systems* (*PEDG*), Aalborg, Denmark, 385-392.
7. Whitehead, J.; Whitehead, J.; Kane, M.; and Zheng, Z. (2022). Exploring public charging infrastructure requirements for short-haul electric trucks. *International Journal of Sustainable Transportation*, 16(9), 775-791.
8. Güney, T. (2019). Renewable energy, non-renewable energy and sustainable development. *International Journal of Sustainable Development and World Ecology*, 26(5), 389-397.

9. Hasan, M.R.; and Mustafi, N.N. (2022). Environmental impacts of the use of electric vehicles. *Environmental Claims Journal*, 34(1), 56-79.
10. Balki, M.K.; Sayin, C.; and Canakci, M. (2014). The effect of different alcohol fuels on the performance, emission and combustion characteristics of a gasoline engine. *Fuel*, 115, 901-906.
11. Monteiro, M.R.; Ambrozin, A.R.P.; Santos, A.O.; Contri, P.P.; and Kuri, S.E. (2010). Evaluation of metallic corrosion caused by alcohol fuel and some contaminants. In *Materials Science Forum*, 636, 1024-1029. Trans Tech Publications Ltd.
12. Komariah, L.N.; Hadiah, F.; Aprianjaya, F.; and Nevriadi, F. (2018). Biodiesel effects on fuel filter; assessment of clogging characteristics. *Proceedings of the 6th International Conference of the Indonesian Chemical Society*, *Journal of Physics*: *Conference Series*, 1095(1), Palembang, South Sumatra, Indonesia, 012017, IOP Publishing.
13. Li, M.; Bai, Y.; Zhang, C.; Song, Y.; Jiang, S.; Grouset, D.; and Zhang, M. (2019). Review on the research of hydrogen storage system fast refueling in fuel cell vehicle. *International Journal of Hydrogen Energy*, 44(21), 10677-10693.
14. Kojima, Y. (2019). Hydrogen storage materials for hydrogen and energy carriers. *International Journal of Hydrogen Energy*, 44(33), 18179-18192.
15. Balitskii, A.; Semerak, M.; Balitska, W.; Subota, A.; and Wus, O. (2015). Hydrogen degradation of the pressure gas tanks materials after long-term service. *Solid State Phenomena*, 225, 39-44.
16. He, M.; Lv, C.; Gong, L.; Wu, J.; Zhu, W.; Zhang, Y.; and Sha, L. (2021). The design and optimization of a cryogenic compressed hydrogen refueling process. *International Journal of Hydrogen Energy*, 46(57), 29391-29399.
17. Poudel, S.; Tun, H.; Reddi, K.; and Elgowainy, A. (2024). Investigation of precooling unit design options in hydrogen refueling station for heavy-duty fuel-cell electric vehicles. *International Journal of Hydrogen Energy*, 61, 493-502.
18. Klopčič, N.; Regenfelder, R.; Hafner, T.; Winkler, F.; Rasche, C.; Rink, M.; and Trattner, A. (2024). Refuelling tests of a hydrogen tank for heavy-duty applications. *International Journal of Hydrogen Energy*, 49, 1237-1249.
19. Fischer, M.S.M.D. (2024). *Experimental and numerical investigations of compressible, transient, and subcritical vessel outflows*. PhD Thesis, Faculty of Bio- and Chemical Engineering of the Technical University of Dortmund.
20. Kadioglu, S.Y.; and Knoll, D.A. (2010). A fully second order implicit/explicit time integration technique for hydrodynamics plus nonlinear heat conduction problems. *Journal of Computational Physics*, 229(9), 3237-3249.
21. Xisto, C.M.; Pascoa, J.C.; Oliveira, P.J.; and Nicolini, D.A. (2010). Implementation of a 3D compressible MHD solver able to model transonic flows. In Pereira, J.C.F.; and Sequeira, A. (Eds.), *Proceedings of the V European Conference on Computational Fluid Dynamics ECCOMAS CFD*, Lisbon, Portugal, 1-14.
22. Boz, Z.; Erdogdu, F.; and Tutar, M. (2014). Effects of mesh refinement, time step size and numerical scheme on the computational modeling of temperature evolution during natural-convection heating. *Journal of Food Engineering*, 123, 8-16.